An asymmetric explosion as the origin of spectral evolution diversity in type Ia Supernovae

K. Maeda[1], S. Benetti[2], M. Stritzinger[3,4], F. K. Röpke[5], G. Folatelli[6], J. Sollerman[7,4],

S. Taubenberger[5], K. Nomoto[1], G. Leloudas[4], M. Hamuy[6], M. Tanaka[1], P. A. Mazzali[5,8],

N. Elias-Rosa[9]

[1]*Institute for the Physics and Mathematics of the Universe (IPMU), University of Tokyo, 5-1-5*

Kashiwanoha, Kashiwa, Chiba 277-8583, Japan: keiichi.maeda@ipmu.jp.

[2]*INAF - Osservatorio Astronomico di Padova, vicolo dell'Osservatorio 5, I-35122 Padova, Italy.*

[3]*Carnegie Institute for Science, Las Campanas Observatory, Colina el Pino Casilla 601, La Serena,*

Chile.

[4]*Dark Cosmology Centre, Niels Bohr Institute, Copenhagen University, Juliane Maries Vej 30,*

2100 Copenhagen Ø, Denmark.

[5]*Max-Planck-Institut für Astrophysik, Karl-Schwarzschild-Straße 1, 85741 Garching, Germany.*

[6]*Universidad de Chile, Departamento de Astronomía, Casilla 36-D, Santiago, Chile.*

[7]*The Oskar Klein Centre, Department of Astronomy, Stockholm University, AlbaNova, 10691*

Stockholm, Sweden.

[8]*Scuola Normale Superiore, Piazza Cavalieri 7, 56127 Pisa, Italy.*

[9]*Spitzer Science Center, California Institute of Technology, 1200 E. California Blvd., Pasadena,*

CA 91125, USA.

1

Type Ia Supernovae (SNe Ia) form an observationally uniform class of stellar explosions, in that more luminous objects have smaller decline-rates[1]. This one-parameter behavior allows SNe Ia to be calibrated as cosmological 'standard candles', and led to the discovery of an accelerating Universe[2,3]. Recent investigations, however, have revealed that the true nature of SNe Ia is more complicated. Theoretically, it has been suggested[4−8] that the initial thermonuclear sparks are ignited at an offset from the centre of the white-dwarf (WD) progenitor, possibly as a result of convection before the explosion[4]. Observationally, the diversity seen in the spectral evolution of SNe Ia beyond the luminosity decline-rate relation is an unresolved issue[9,10]. Here we report that the spectral diversity is a consequence of random directions from which an asymmetric explosion is viewed. Our findings suggest that the spectral evolution diversity is no longer a concern in using SNe Ia as cosmological standard candles. Furthermore, this indicates that ignition at an offset from the centre of is a generic feature of SNe Ia.

When a carbon-oxygen WD reaches a critical limit known as the Chandrasekhar mass ($\sim$ 1.38 $M_\odot$), its central density and temperature increase to a point where a thermonuclear runaway is initiated. The thermonuclear sparks give birth to a subsonic deflagration flame, which at some point may make a transition to a supersonic detonation wave that leads to the complete disruption of the WD[11,12]. The thermalization of γ-rays produced from the decay of freshly synthesized radioactive ^{56}Ni powers the transient source, known as a SN Ia[13,14]. The relationship between the luminosity and the decline-rate parameter ($\Delta m_{15}(B)$, which is the difference between the B-band magnitude at peak and that measured 15 days later) is interpreted to be linked to the amount of newly synthesized ^{56}Ni (refs. 15, 16).

SNe Ia displaying a nearly identical photometric evolution can exhibit appreciably different expansion velocity gradients ($\dot{v}_{Si}$) as inferred from the Si II λ6355 absorption feature[10,17]. More specifically, objects that show $\dot{v}_{Si} \gtrsim 70$ km s^{-1} day^{-1} are placed into the high-velocity gradient (HVG) group, while those that show smaller gradients are placed in the low-velocity gradient (LVG) group. For normal SNe Ia[18], which are the predominant population of the total SN Ia sample and the main focus of this *Letter*, $\dot{v}_{Si}$ is *not* correlated with $\Delta m_{15}(B)$ (ref. 10; Fig. 1a, 1b), thus raising a nagging concern regarding the 'one-parameter' description.

Late phase nebular spectra can be used to trace the distribution of the inner ejecta[19]. Beginning roughly half a year after explosion, as the ejecta expands, its density decreases to the point where photons freely escape. Photons originating from the near/far side of the ejecta are detected at a shorter/longer (blue-shifted/red-shifted) wavelength because of Doppler shifts. For SNe Ia,

emission lines related to [Fe II] $\lambda 7155$ and [Ni II] $\lambda 7378$ are particularly useful, as they are formed in the ashes of the deflagration flame[19]. These lines show diversity in their central wavelengths – blue-shifted in some SNe Ia and red-shifted in others (see Fig. 1c) – which provides evidence that the deflagration ashes, therefore the initial sparks, are on average located off-centre. The wavelength shift can be translated to a line-of-sight velocity ($v_{\rm neb}$) of the deflagration ashes.

Figure 2 shows a comparison between $\dot{v}_{\rm Si}$ and $v_{\rm neb}$ for 20 SNe Ia. Details regarding the data are provided in SI §1. Although the diversities in these observables were discovered independently, Fig. 2 clearly shows that they are connected. Omitting the peculiar SN 2004dt (Fig. 2 Legend; SI §1), all 6 HVG SNe show $v_{\rm neb} > 0$ km s^{-1} (i.e., red-shifts), which means that these events are viewed from the direction opposite to the off-centre initial sparks. The 11 LVGs display a wider distribution in $v_{\rm neb}$ space, but are concentrated to negative values (i.e., blue-shifted), indicating that these events are preferentially viewed from the direction of the initial sparks. If HVG and LVG SNe were intrinsically distributed homogeneously as a function of $v_{\rm neb}$, the probability that just by chance (as a statistical fluctuation) all HVG SNe show $v_{\rm neb} > 0$ km s^{-1} is merely 0.4%; it is thus quite unlikely. Indeed, the probability that by chance 6 HVG SNe are among the 7 SNe showing the largest red-shift in $v_{\rm neb}$ in our sample of 17 SNe is only 0.06%.

This finding strongly indicates that HVG and LVG SNe do not have intrinsic differences, but that this diversity arises solely from a viewing angle effect. Figure 3 shows a schematic picture. If viewed from the direction of the off-centre initial sparks, an SN Ia appears as an LVG event at early phases and shows blue-shifts in the late-time emission-lines. If viewed from the opposite

direction, it appears as an HVG event, and shows red-shifts at late phases.

The number of HVG SNe is $\sim 35\%$[10] of the total number of HVG and LVG SNe. To explain this, the angle to the observer at which an SN changes its appearance from an LVG to an HVG is $\sim 105 - 110°$, measured relative to the direction between the centre and the initial sparks. The velocity shift of $3,500$ km s^{-1} in the distribution of the deflagration ashes, as derived for the normal SN Ia 2003hv through a detailed spectral analysis[19], corresponds to $v_{\mathrm{neb}} \sim 1000$ km s^{-1} if viewed from this transition angle. The configuration then predicts that all LVG SNe should show $-3,500 < v_{\mathrm{neb}} < 1000$ km s^{-1}, while all HVG SNe should be in the range $1000 < v_{\mathrm{neb}} < 3,500$ km s^{-1}. These ranges are shown as arrows in Fig. 2, and provide a good match to the observations.

Figure 4a shows an example of a hydrodynamic model in which the thermonuclear sparks were ignited off-centre in a Chandrasekhar-mass WD[6] (an alternative way of introducing global asymmetries is double detonations in sub-Chandrasekhar-mass WDs[20]). Although this model has not been fine-tuned to reproduce the present finding, it does have the required generic features. The density distribution is shallow and extends to high velocity in the direction opposite to the initial sparks (Fig. 4b). Initially, the photosphere is at high velocity if viewed from this direction, as the region at the outer, highest velocities is still opaque. Later on, the photosphere recedes inwards faster in this opposite direction, owing to the shallower density gradient. As a result, the SN looks like an LVG if viewed from the offset direction, but like an HVG SN from the opposite direction (Fig. 4c), as in our proposed picture (Fig. 3).

Our finding provides not only strong support for the asymmetric explosion as a generic fea-

5

ture, but also constraints on the still-debated deflagration-to-detonation transition. In this particular simulation, the change in appearance (as an HVG or an LVG SN) takes place rather abruptly around the viewing direction of $\sim 140°$. Owing to the offset ignition, the deflagration flame propagates asymmetrically and forms an off-centre, shell-like region of high density deflagration ash. The detonation is ignited at an offset following the deflagration, but tries to expand almost isotropically. However, the angle between $0°$ and $140°$ is covered by the deflagration ash, into which the strong detonation wave (fueled by the unburned material near the centre of the WD) cannot penetrate. On the other hand, in the $140 - 180°$ direction, the detonation can expand freely, creating a shallow density distribution. The 'abrupt' change in appearance, as inferred by the observational data, is therefore a direct consequence of the offset models, controlled by the distribution of the deflagration ash. The 'opening angle' of the transition is on the other hand dependent on the details of the explosion. To accurately model this according to our finding ($\sim 105 - 110°$ for the typical transition angle), either a smaller offset of the initial deflagration sparks or an earlier deflagration-to-detonation transition would be necessary. Such changes are also required to produce the typical velocity shift of $\sim 3,500$ km s^{-1} in the distribution of the deflagration ash.

Our proposed model unifies into a single scheme recent advances in both theoretical and observational studies of SNe Ia - and it does not conflict with other results produced by spectral tomography[16,21] or polarization measurements[22] (SI §2). Our interpretation suggests that two SNe with very similar light curve evolution may not necessarily produce exactly the same amount of ^{56}Ni. They might in fact show somewhat different light curve evolution if viewed from the same direction (relative to the offset between the centre and the initial sparks), but the light curves look

the same to an observer as $\Delta \mathrm{m}_{15}(B)$ can change with viewing direction[5] (SI §3). This situation is a natural consequence of observing a number of SNe Ia with a large variation in ^{56}Ni production and in the viewing angles. Our finding regarding the explosion mechanism will lead to quantitative evaluation on the contribution of this random effect to the observed scatter in the SN Ia luminosities beyond the one-parameter description[5], as compared to other systematic effects, such as the stellar environment[23].

1. Phillips, M. M., et al., The Reddening-Free Decline Rate Versus Luminosity Relationship for Type Ia Supernovae, Astron. J., **118**, 1766-1776 (1999)

2. Permutter, S., et al., Measurements of Ω and Λ from 42 High-Redshift Supernovae, Astrophys. J., **517**, 565-586 (1999)

3. Riess, A., et al., Observational Evidence from Supernovae for an Accelerating Universe and a Cosmological Constant, Astron. J., **116**, 1009-1038 (1998)

4. Kuhlen, M., Woosley, S. E., & Glatzmaier, G. A., Carbon Ignition in Type Ia Supernovae. II. A Three-dimensional Numerical Model, Astrophys. J., **640**, 407-416 (2006)

5. Kasen, D., Röpke, F. K., & Woosley, S. E., The Diversity of Type Ia Supernovae from Broken Symmetries, Nature, **460**, 869-872 (2009)

6. Maeda, K., et al., Nucleosynthesis in Two-Dimensional Delayed Detonation Models of Type Ia Supernova Explosions, Astrophys. J., **712**, 624-638 (2010)

7. Röpke, F. K., Woosley, S. E., & Hillebrandt, W., Off-Center Ignition in Type Ia Supernovae. I. Initial Evolution and Implications for Delayed Detonation, Astrophys. J., **660**, 1344-1356 (2007)

8. Jordan, G. C., et al., Three-Dimensional Simulations of the Deflagration Phase of the Gravitationally Confined Detonation Model of Type Ia Supernovae, Astrophys. J., **681**, 1448-1457 (2008)

9. Branch, D., Drucker, W., & Jeffery, D. J., Differences among Expansion Velocities of Type Ia Supernovae, Astrophys. J., **330**, L117-L118 (1988)

10. Benetti, S., et al., The Diversity of Type Ia Supernovae: Evidence for Systematics?, Astrophys. J., **623**, 1011-1016 (2005)

11. Khokhlov, A. M., Delayed Detonation Model for Type Ia Supernovae, Astron. Astrophys. **245**, 114-128 (1991)

12. Iwamoto, K., et al., Nucleosynthesis in Chandrasekhar Mass Models for Type Ia Supernovae and Constraints on Progenitor Systems and Burning-Front Propagation, Astrophys. J. Suppl. **125**, 439-462 (1999)

13. Nomoto, K., Thielemann, F.-K., & Yokoi, K., Accreting White Dwarf Models of Type I Supernovae. III - Carbon Deflagration Supernovae, Astrophys. J., **286**, 644-658 (1984)

14. Woosley, S. E., & Weaver, T. A., The Physics of Supernova Explosions, Ann. Rev. Astron. Astrophys., **24**, 205-253 (1986)

15. Höflich, P., et al., Maximum Brightness and Postmaximum Decline of Light Curves of Type Ia Supernovae: A Comparison of Theory and Observations, Astrophys. J., **472**, L81-L84 (1996)

16. Mazzali, P. A., Röpke, F. K., Benetti, S., & Hillebrandt, W., A Common Explosion Mechanism for Type Ia Supernovae, Science, **315**, 825-828 (2007)

17. Benetti, S., et al., Supernova 2002bo: Inadequacy of The Single Parameter Description, Mon. Not. R. Astron. Soc., **348**, 261-278 (2004)

18. Branch, D., Fisher, A., & Nugent, P., On The Relative Frequencies of Spectroscopically Normal and Peculiar Type Ia Supernovae, Astron. J., **106**, 2383-2391 (1993)

19. Maeda, K., et al., Nebular Spectra and Explosion Asymmetry of Type Ia Supernovae, Astrophys. J., **708**, 1703-1715 (2010)

20. Fink, M., Röpke, F. K., Hillebrandt, W., Seitenzahl, I. R., Sim, S. A., & Kromer, M., Double-Detonation Sub-Chandrasekhar Supernovae: Can Minimum Helium Shell Masses Detonate The Core?, Astron. Astrophys., **514**, 53-62 (2010)

21. Stehle, M., Mazzali, P.A., Benetti, S., & Hillebrandt, W., Abundance Stratification in Type Ia Supernovae - I. The Case for SN 2002bo, Mon. Not. R. Astron. Soc., **360**, 1231-1243 (2005)

22. Wang, L., Baade, D., & Patat, F., Spectropolarimetric Diagnostics of Thermonuclear Supernova Explosions, Science, **315**, 212-214 (2007)

23. Neill, J. D., et al., The Local Hosts of Type Ia Supernovae, Astrophys. J., **707**, 1449-1465 (2009)

24. Jha, S., et al., The Type Ia Supernova 1998bu in M96 and The Hubble Constant, Astrophys. J. Suppl., **125**, 73-97 (1999)

25. Cappellaro, E., et al., Detection of a Light Echo from SN 1998bu, Astrophys. J., **549**, L215-L218 (2001)

26. Filippenko, A. V., et al., The Subluminous, Spectroscopically Peculiar Type Ia Supernova 1991bg in The Elliptical Galaxy NGC 4374, Astron. J., **104**, 1543-1556 (1992)

27. Turatto, M., et al., The Properties of The Peculiar Type Ia Supernova 1991bg. I. Analysis and Discussion of Two Years of Observations, Mon. Not. R. Astron. Sco., **283**, 1-17 (1996)

28. Morrell, N., Folatelli, G., & Stritzinger, M., Supernova 2007on In NGC 1404, CBET, **1131** (2007)

29. Altavilla, G., et al., The Early Spectral Evolution of SN 2004dt, Astron. Astrophys., **475**, 585-595 (2007)

30. Wang, X., et al., Improved Distances to Type Ia Supernovae with Two Spectroscopic Sub-classes, Astrophys. J., **699**, L139-L143 (2009)

Author Contributions   S.B. and K.M. found the relation between the velocity gradient and the nebular velocity, initiated and organized the project. K.M. wrote the manuscript with the assistance of M.S., J.S., G.F., and S.T. S.B. is responsible for the late-phase spectrum of SNe 1997bp. M.S., G.F., and M.H are responsible for acquisition and reduction of SNe 2007on, 2007sr, and 2009ab. F.K.R. and K.M. are responsible for the explosion simulation. All the authors contributed to discussions.

Competing Interests   The authors declare that they have no competing financial interests.

Correspondence   Correspondence and requests for materials should be addressed to K.M. (email: keiichi.maeda@ipmu.jp).

(a)

02bo

98bu (+ 1.8 mag)

Days since *B*-band maximum

B-band Magnitude

(b)

02bo −4

98bu −4

02bo +28

98bu +28

Nomalized Flux

v_{si} [km s^{-1}]

(c)

[Fe II] $\lambda 7155$

[Ni II] $\lambda 7378$

02bo +368

98bu +249

Normalized Flux

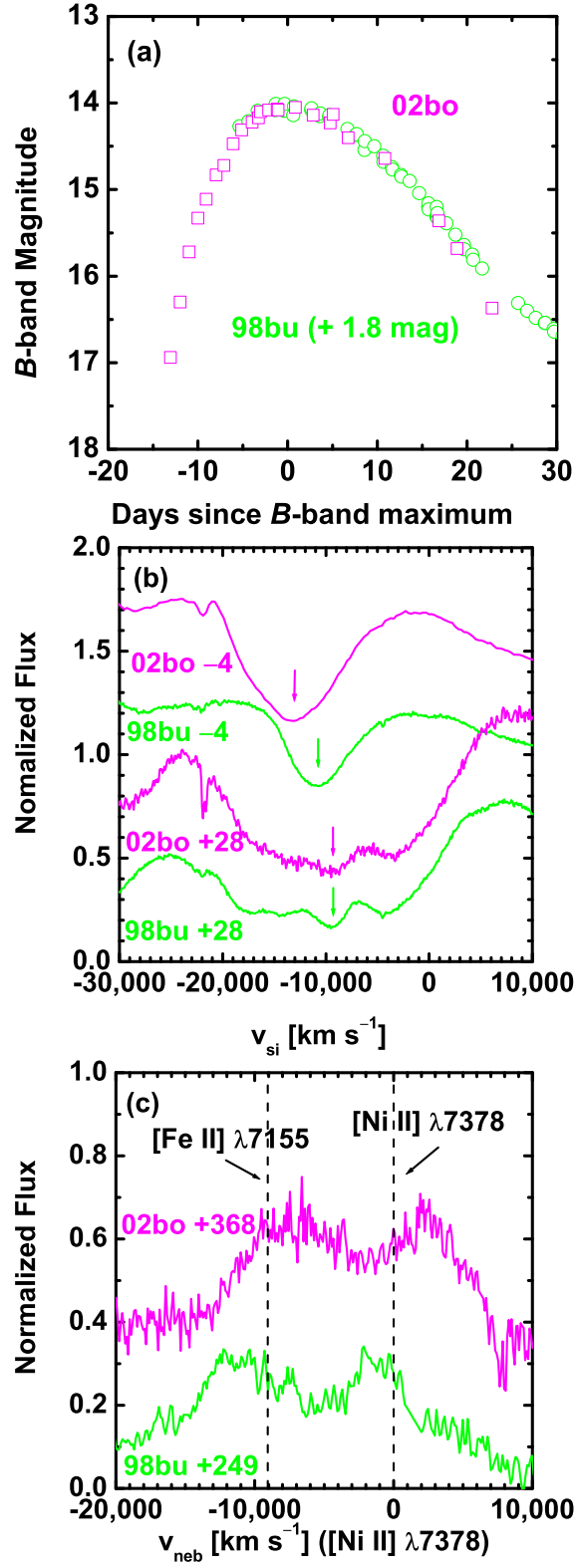v_{neb} [km s^{-1}] ([Ni II] $\lambda 7378$)

Figure 1   **Comparison between HVG SN Ia 2002bo and LVG SN Ia 1998bu.**   The

decline-rate parameter $\Delta\mathrm{m}_{15}(B)$ is 1.16 and 1.06 mag for SNe 2002bo and 1998bu, re-

spectively. **a.** The B-band light curves[17,24]. The magnitudes for SN 1998bu have been

artificially shifted in the y-direction for presentation. **b.** Si II $\lambda6355$ at different epochs[17,24]

(in days with respect to B-band maximum). SN 2002bo had initially a larger absorption

velocity than SN 1998bu, but later its velocity approached that of SN 1998bu. The velocity

evolved quicker and the velocity gradient ($\dot{v}_{\mathrm{Si}}$) is larger for SN 2002bo than for SN 1998bu.

c. [Fe II] $\lambda7155$ and [Ni II] $\lambda7378$ in late-time spectra[21,25]. The horizontal axis denotes the

line velocity measured from the rest wavelength of [Ni II] $\lambda7378$. The rest wavelengths of

[Fe II] $\lambda7155$ and [Ni II] $\lambda7378$ are marked by dashed lines. These lines are red-shifted

in SN 2002bo while blue-shifted in SN 1998bu. The wavelength shift indicates the line-

of-sight velocity of the deflagration ashes (v_{neb}) ($v_{\mathrm{neb}} < 0$ km s^{-1}, i.e., the blue-shift, if the

material is moving toward us). These are the strongest lines among those emitted from

the deflagration ash according to the previous analysis of late-time emission lines[19]. In-

deed, there are stronger lines which do not show Doppler shifts, e.g., [Fe III] $\lambda4701$; they

however do not trace the distribution of the deflagration ash[19] (see also SI §1) and are

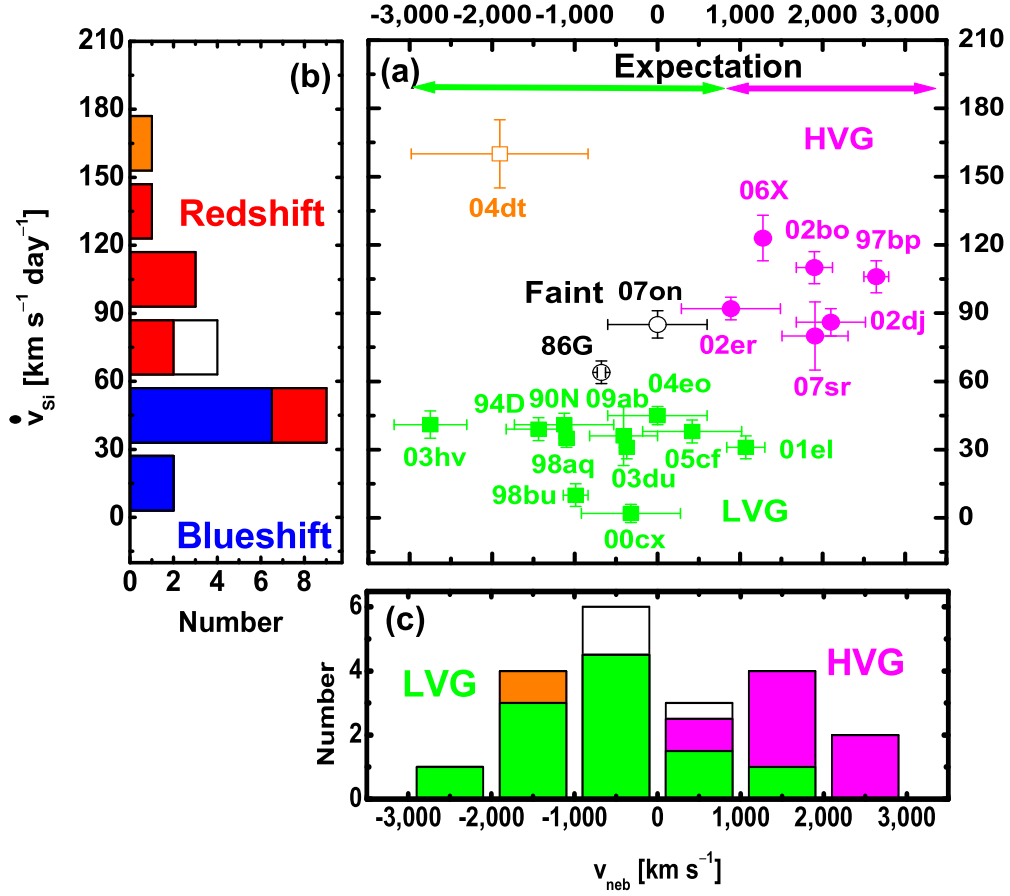thus not useful in the present study.

Figure 2   **Relations between the features in early- and late-phases.**   **a.** Early-phase velocity gradient ($\dot{v}_{Si}$: vertical axis) as compared to late-phase emission-line shift velocity (v_{neb}: horizontal axis) for 20 SNe Ia. The errors are for 1σ in fitting the velocity evolution for $\dot{v}_{Si}$, while for v_{neb} the errors are from differences in measurement between different emission lines (see Sup §1). LVG SNe and HVG SNe are shown by green squares and magenta circles, respectively. SNe 1986G and 2007on are classified as 'faint and fast-declining' SNe Ia[26−28] (black open circles). SN 2004dt (orange square) is an HVG SN according to the value of $\dot{v}_{Si}$, but displayed peculiarities in the late-time spectrum[29] (SI §1) and in polarization measurements[22] (SI §2), and the value for $\dot{v}_{Si}$ is exceptionally large

14

as compared to other HVG SNe. These suggest that SN 2004dt is an outlier and the origin of its large $\dot{v}_{\mathrm{Si}}$ is probably different from that of other SNe Ia. The two arrows on top indicate the regions where HVG and LVG SNe are expected, based on a simple kinematic interpretation (see main text). **b.** Number distribution of 20 SNe as a function of $\dot{v}_{\mathrm{Si}}$. White and orange areas are for faint SNe and SN 2004dt. The remaining SNe are marked depending on whether they show a blue-shift ($v_{\mathrm{neb}} < 0$ km s^{-1}: blue area) or red-shift ($v_{\mathrm{neb}} > 0$ km s^{-1}: red area) in their late-time spectra. **c.** Number distribution of 20 SNe as a function of v_{neb}.
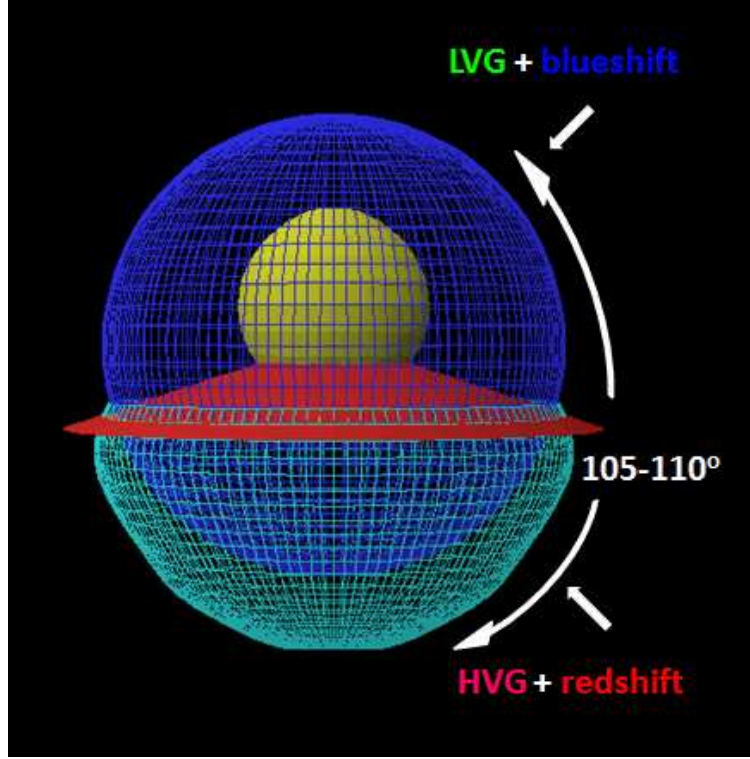
Figure 3   **A schematic picture of the structure of SN Ia ejecta.**   This configuration

simultaneously explains the relative fractions of HVG and LVG SNe Ia, and the relation

between $\dot{v}_{\mathrm{Si}}$ and v_{neb}. It is also consistent with the diversity in v_{neb} (ref. 19). The ashes

of the initial deflagration sparks are shifted with respect to the center of the SN ejecta by

$\sim 3,500$ km s^{-1} (yellow: Although expressed by a spherical region for presentation, it may

well have an amorphous shape owing to the hydrodynamic instability in the deflagration

flame[7]). This region is rich in stable ^{58}Ni with a small amount of radioactive ^{56}Ni, and emits

[Fe II] λ7155 and [Ni II] λ7378 at late phases[19] (SI §1). The outer region is the later deto-

nation ash responsible for the early-phase Si II λ6355 absorption. This region is roughly

spherically distributed (blue), but extends to the outer region in the direction opposite to

the deflagration ashes (cyan). Although the detonation can produce ^{56}Ni which decays into ^{56}Fe, it has been argued that these regions (blue and cyan) are not main contributors to [Fe II] λ7155 and [Ni II] λ7378 at late phases[19] (SI §1). A putative observer would view this explosion as an LVG or HVG SN, depending on the direction of the observer, as divided by a specific angle (red), which is $\sim 105 - 110°$. This angle is derived from the relative numbers of HVG and LVG SNe (see main text); the fraction of HVG SNe to the total number of HVG and LVG SNe $\sim 35\%$ (ref. 10), as was also supported by a larger sample[30] with more than 100 SNe (using the observed trend that the HVG SNe show higher velocities than LVG objects at early times).
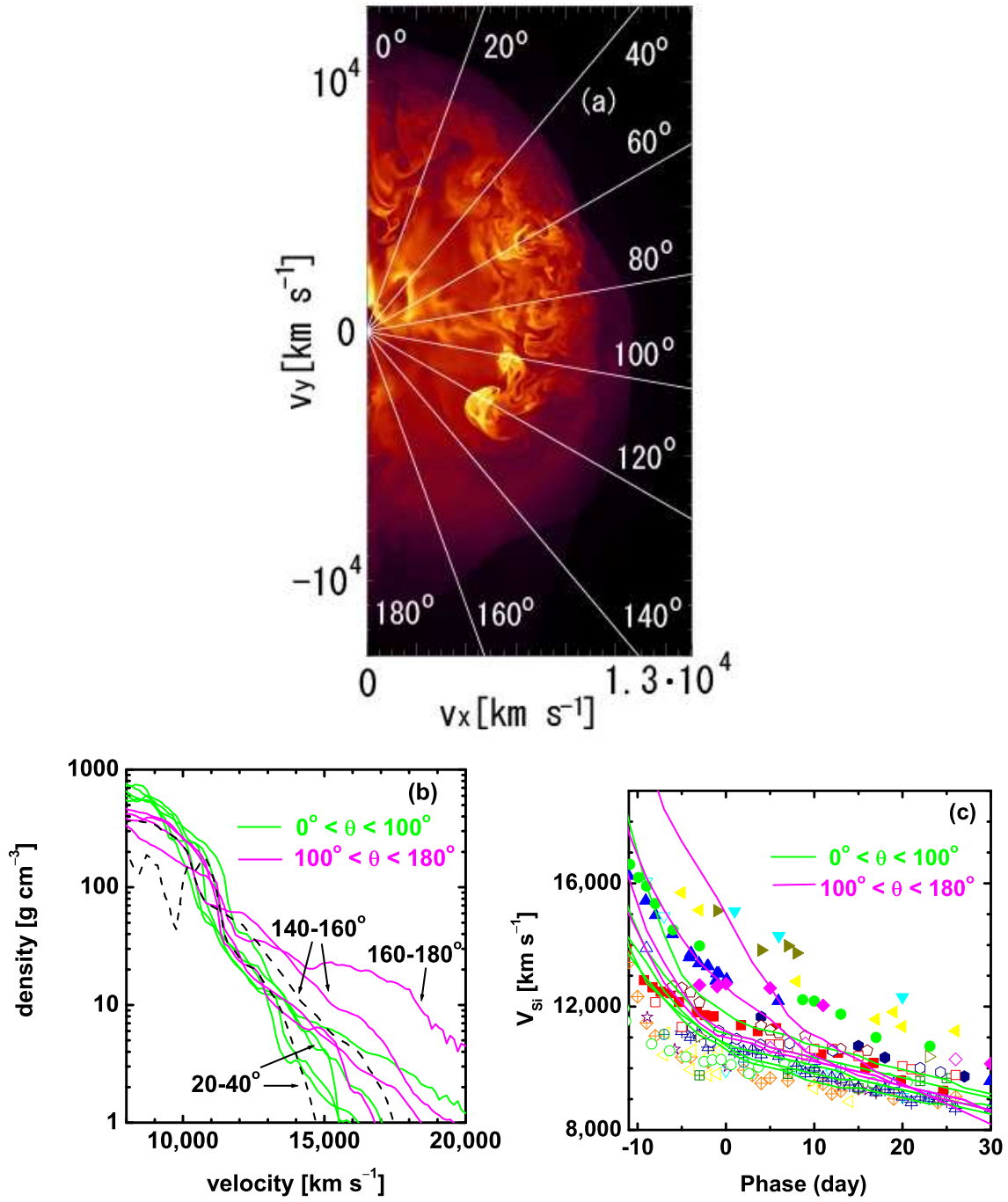
Figure 4 **Expectations from a hydrodynamic explosion model. a.** Cross section of the

density distribution of an offset ignition model[6] (similar to a model in ref. 5). It is shown

at 10 seconds after the ignition, when the homologous expansion is already reached. In this model, the deflagration sparks were ignited offset, within an opening angle of $45°$ and between $0 - 180$ km from the centre of a WD whose radius is $\sim 2,000$ km. The deflagration products are distributed in the high-density offset shell, which covers $0 - 140°$ in this particular model. This resulting velocity shift is $\sim 8,000$ km s^{-1} in this model, which is larger than the observational requirement ($\sim 3,500$ km s^{-1}). **b.** Radial density distribution of the same model for several directions (where the angle is measured from the direction of the offset sparks). The magenta lines show the density distribution for the angle in $100 - 180°$, roughly corresponding to the putative directions for which a SN looks like an HVG SN inferred from the observational data (Fig. 3). Also shown is the density distribution multiplied by the mass fraction of Intermediate mass elements, which gives a rough distribution of Si, for two directions ($20 - 40°$ and $140 - 160°$). It is seen that the distribution of Si roughly follows the density distribution. **c.** Model photospheric velocity evolution for several directions (lines) as compared to the observed Si II $\lambda 6355$ absorption line evolution[10] (filled and open symbols for HVG and LVG SNe, respectively; the phase in days with respect to B-band maximum). The position of the photosphere is estimated by integrating the optical depth with a constant opacity along each direction. Using the Si distribution for the velocity estimate provides a similar result.

Supplementary Information

1 Supernova Sample and Notes for Individual SNe

Supplementary Table 1 summarizes the data of the SNe used in the present study. The values of the velocity gradients ($\dot{v}_{\mathrm{Si}}$) are obtained from the literature when available. They are mostly drawn from a previous compilation[10] (see Supplementary Tab. 1 for the sources of the observations), with values for additional SNe obtained from the references listed in Supplementary Table 1. For SN 1998aq, we have measured $\dot{v}_{\mathrm{Si}}$ from the published spectra[38].

The line-of-sight velocity of the deflagration ash is derived as follows. Late-time spectra of SNe Ia show various forbidden lines from Fe-peak elements. These lines can be divided into two groups. The first group requires intense heating from radioactive ^{56}Ni $\rightarrow$ ^{56}Co $\rightarrow$ ^{56}Fe decays and low material density (e.g., [Fe III] $\lambda 4701$), while the second group requires a low heating rate and high material density (e.g., [Fe II] $\lambda 7155$ and [Ni II] $\lambda 7378$). Considering general properties of the emission process[19], the former lines are argued to be preferentially emitted from the detonation ash (because it is at relatively low density with a large amount of ^{56}Ni), while the latter lines are formed in the deflagration ash (because it is at high density with a small amount of ^{56}Ni). These two groups of lines show mutually different properties in observations, strengthening the interpretation that they are emitted from different regions: The 'deflagration ash'-lines show the diversity in Doppler

shift (not only in [Fe II] $\lambda7155$ and [Ni II] $\lambda7378$[61,62]), while the 'detonation ash'-lines show virtually no Doppler shifts. This property led to the conclusion that the deflagration ash is on average located offset, while the detonation ash is distributed roughly spherically[19].

For v_{neb} (the line-of-sight velocity of the deflagration ash), we have therefore measured the wavelength shift in [Ni II] $\lambda7378$ and in [Fe II] $\lambda7155$, and defined v_{neb} as the mean value of them (see Supplementary Tab. 1 for the source of the observational data). The error bars are taken to be the difference in the measurements for the two lines. In all SNe except for SN 2004dt, the difference in these two measurements is at most 600 km s^{-1}. For SNe Ia in which either of [Fe II] $\lambda7155$ or [Ni II] $\lambda7378$ is weak and unidentified, we measure v_{neb} only from the other single line, with a conservative error of 600 km s^{-1}. For SNe 2007on, 2007sr, and 2009ab, we have measured $\dot{v}_{\mathrm{Si}}$ and v_{neb} from our own spectra taken at the Gemini South, the Magellan, and the ESO (La Silla, Paranal) telescopes. The late-time spectrum of SNe 1997bp has also been obtained by us and used to measure v_{neb}. The 20 SNe in Supplementary Table 1 are all the objects we have found for which both $\dot{v}_{\mathrm{Si}}$ and v_{neb} are reliably available to date. Also shown in the table are the light-curve decline-rate parameters $\Delta m_{15}(B)$.

Supplementary Table 1 also lists the epoch (after B-band maximum) of the late-time spectra from which v_{neb} is measured. For most of the SNe Ia, it is at least 200 days after B-band maximum, and thus errors caused by the blending of additional lines to this feature (e.g., permitted lines emitted at relatively early phases) in measuring v_{neb} can be

avoided. The features at $\sim 7,000 - 7,500$ Å, which we interpret to be dominated by [Fe II] $\lambda7155$ and [Ni II] $\lambda7378$, do not show significant evolution at $\gtrsim 100 - 150$ days after B-band maximum[19].

It has been shown that normal SNe Ia[18] (which constitute $\gtrsim 80\%$ of the whole SN Ia population), faint 1991-bg like SNe Ia[26], and bright 1991T-like SNe Ia[63,64] show different properties in $\dot{v}_{\mathrm{Si}}$[10]. Normal SNe Ia show a diversity in $\dot{v}_{\mathrm{Si}}$, which is apparently *not* correlated with $\Delta m_{15}(B)$. Faint 1991bg-like SNe Ia, which are characterized by a rapid fading (i.e., large $\Delta m_{15}(B)$), always show large $\dot{v}_{\mathrm{Si}}$. Bright 1991T-like SNe Ia with small $\Delta m_{15}(B)$ always show small $\dot{v}_{\mathrm{Si}}$. In deriving v_{neb}, we have noticed that the identification of [Fe II] $\lambda7155$ and [Ni II] $\lambda7378$ is robust for normal SNe Ia, but tends to be a subject of possible misidentification for the other subclasses (then such SNe Ia are omitted from our analysis): Faint 1991bg-like SNe Ia tend to show probable [Ca II] $\lambda7291$, 7324 [27]. Bright 1991T-like SNe Ia tend to show a broad single peak, possibly indicating that [Fe II] $\lambda7155$ and [Ni II] $\lambda7378$ are broad and mutually blended. These indicate that the ejecta structure (density, temperature, and composition) of faint and bright SNe Ia is intrinsically different from normal ones. This is a reason why our sample is mainly composed of normal SNe Ia. Luckily, omitting a large fraction of faint/bright SNe Ia is not important for our present analysis, since we are interested in the spectral diversity beyond the one-parameter $\Delta m_{15}(B)$ description, which is a problem only in normal SNe Ia.

For normal SNe Ia, we categorize HVG SNe and LVG SNe according to $\dot{v}_{\mathrm{Si}}$, with the

division line at 70 km s^{-1} day^{-1}. According to its $\dot{v}_{\mathrm{Si}}$, SN 2004dt is an HVG. However, its peculiar observational features suggest that it is an outlier, and the origins of its high velocity gradient and the negative v_{neb} are likely different than the one for other HVGs (see Fig. 2 caption). One of the peculiar features of SN 2004dt appears in its late-time spectra. Supplementary Fig. 1 shows a late-time spectrum of SN 2004dt compared to the prototypical faint SN 1991bg and to the normal HVG SN 2007sr. The spectrum of SN 2004dt provides a good match to that of the faint SN 1991bg. Both the intensity and the width of the lines at $\sim 7,000 - 7,500$ Å are similar for these two SNe. In normal HVG SN 2007sr, the features at $7,000 - 7,500$ Å are much fainter than for SNe 2004dt and 1991bg. This indicates that in the case of SN 2004dt the feature is probably contaminated by other lines, most likely [Ca II] $\lambda\lambda7291, 7324$ (note that SN 2004dt shows a larger error in v_{neb} than the other SNe Ia). In addition, the strongest lines at late phases, i.e., the [Fe III] blend at $\sim 4,700$ Å and the [Fe II] and [Fe III] blend at $\sim 5,250$ Å have similar ratios in SN 2004dt and 1991bg; these ratios have been noticed to be peculiar[29]. The normal HVG SN 2007sr has broader lines, and different line ratios. These similarities between the 'normal' SN 2004dt and the faint SN 1991bg at late phases, which have not been noticed previously, suggest that these explosions might be closely related to one another. SN 2004dt may represent a new class of SNe Ia[65] which have SN 1991bg-like features in the late-time spectrum, but are more energetic and brighter.

Supplementary Table 1: Supernovae Sample

SN	$\Delta m_{15}(B)$	$\dot{v}_{\mathrm{Si}}$ (km s^{-1} day^{-1})	v_{neb} (km s^{-1})	Epoch (day)	Class[8,24]	References
1986G	1.81 ± 0.07	64 ± 5	-680 ± 50	257	HVG/Faint	1, 31, 32
1990N	1.07 ± 0.05	41 ± 5	-1130 ± 600	280	LVG	1, 10, 33, 34
1994D	1.32 ± 0.05	39 ± 5	-1440 ± 390	306	LVG	1, 34, 35
1997bp	0.97 ± 0.2	106 ± 7	2650 ± 150	300	HVG	10, 36
1998aq	1.12 ± 0.05	35 ± 4	-1100 ± 50	241	LVG	37, 38
1998bu	1.06 ± 0.05	10 ± 5	-990 ± 150	329	LVG	1, 10, 24, 25, 39
2000cx	0.93 ± 0.04	2 ± 4	-320 ± 600	147	LVG/peculiar	40-43
2001el	1.13 ± 0.04	31 ± 5	1070 ± 230	398	LVG	44-46
2002bo	1.16 ± 0.06	110 ± 7	1900 ± 220	368	HVG	17, 21
2002dj	1.08 ± 0.05	86 ± 6	2100 ± 420	275	HVG	47
2002er	1.32 ± 0.03	92 ± 5	890 ± 600	216	HVG	48, 49
2003du	1.02 ± 0.05	31 ± 5	-370 ± 50	377	LVG	50, 51
2003hv	1.61 ± 0.02	41 ± 6	-2750 ± 440	320	LVG	52
2004dt	1.21 ± 0.05	160 ± 15	-1910 ± 1070	152	HVG/peculiar	29
2004eo	1.45 ± 0.04	45 ± 4	0 ± 600	228	LVG	53, 54
2005cf	1.12 ± 0.03	35 ± 5	420 ± 600	267	LVG	55-58
2006X	1.31 ± 0.05	123 ± 10	1280 ± 20	277	HVG	59
2007on	1.62 ± 0.01	85 ± 6	0 ± 600	356	HVG/Faint	This work
2007sr	0.93 ± 0.02	80 ± 15	1910 ± 400	256	HVG	60
2009ab	1.20 ± 0.02	36 ± 13	-410 ± 410	278	LVG	This work

2 Other Observational Constraints

In abundance 'tomography'[16,21,66−68], a temporal sequence of spectra of individual SNe Ia are used to infer the distribution of different elements through the SN ejecta, assuming the density structure of a spherically symmetric explosion model[13]. From this type of analysis, it has been indicated that the abundance distribution is generally a function of $\Delta m_{15}(B)$. The difference between the HVG and LVG SNe, not related to $\Delta m_{15}(B)$, is mainly on the extent of the Si-rich layer[16] and on the photospheric velocity[66], which are explained by our proposed scenario (main text).

On the other hand, the spatial extent of the ^{56}Ni-rich region does not seem to be dependent on whether it is a HVG or a LVG SN[16]. This could provide a constraint on the ejecta asymmetry. In the offset explosion model, the spatial extent of the ^{56}Ni region, as well as the density structure at the outer edge of that region, are not sensitive to the direction, despite the initially large asymmetry in the ignition[6]. This stems from the nature of the propagation of the detonation wave as described in the main text; unlike the deflagration flame, the detonation tries to expand isotropically, producing roughly spherically distributed ^{56}Ni. This region is not sensitively affected by the existence of the deflagration ashes, which is essential in determining the structure of Si-rich region. As a result, the spatial extent of the ^{56}Ni-rich region is mainly controlled by the different amounts of ^{56}Ni produced in the explosion, and the viewing angle dependence could add some diversity at most as a secondary effect[6]; this is consistent with the observational indications[16].

The asymmetric distribution of the outermost layer may imprint its signature in polarization measurements, which may be linked to the velocity gradient[69]. The polarization of the Si II line is correlated with $\Delta m_{15}(B)$[22], but only for LVG SNe (Supplementary Fig. 2). HVG SNe generally show larger polarization than LVG SNe[70,71] but they clearly do not follow this trend. A global one-sided asymmetry as in the present interpretation would produce relatively low continuum polarization and relatively high line polarization at Si II $\lambda6355$[72]. In our proposed scenario the global asymmetry is of smaller degree than in an extremely asymmetric model producing Si II polarization of $\sim 1\%$[72], thus this is likely not a major contributor to the observed polarization. Alternatively, it has been suggested, based on the correlation between the Si II polarization and $\Delta m_{15}(B)$, that the observed Si II polarization could be a measure of the thickness of the outer layer above the ^{56}Ni-rich region, in which the local inhomogeneity, e.g., a few relatively dense blobs, is assumed to be a source of polarization. In this interpretation, the large Si II polarization in HVG SNe could be a consequence of an extended outer layer in the direction opposite to the initial sparks.

3 Viewing-Angle Effect on the Light Curve

It has been suggested that if the ejecta are asymmetric, $\Delta m_{15}(B)$ is dependent on the direction to the observer[5]. Supplementary Fig. 3 shows the comparison between $\Delta m_{15}(B)$ and v_{neb} for SNe Ia.

In the same figure, the possible effect of the viewing angle on the light curve shape, and the implication on the scatter in the luminosity calibration beyond the one-parameter description, are schematically illustrated. For example, the LVG SN 1998bu and the HVG SN 2002bo had similar $\Delta m_{15}(B)$ values, and this could be interpreted as follows.
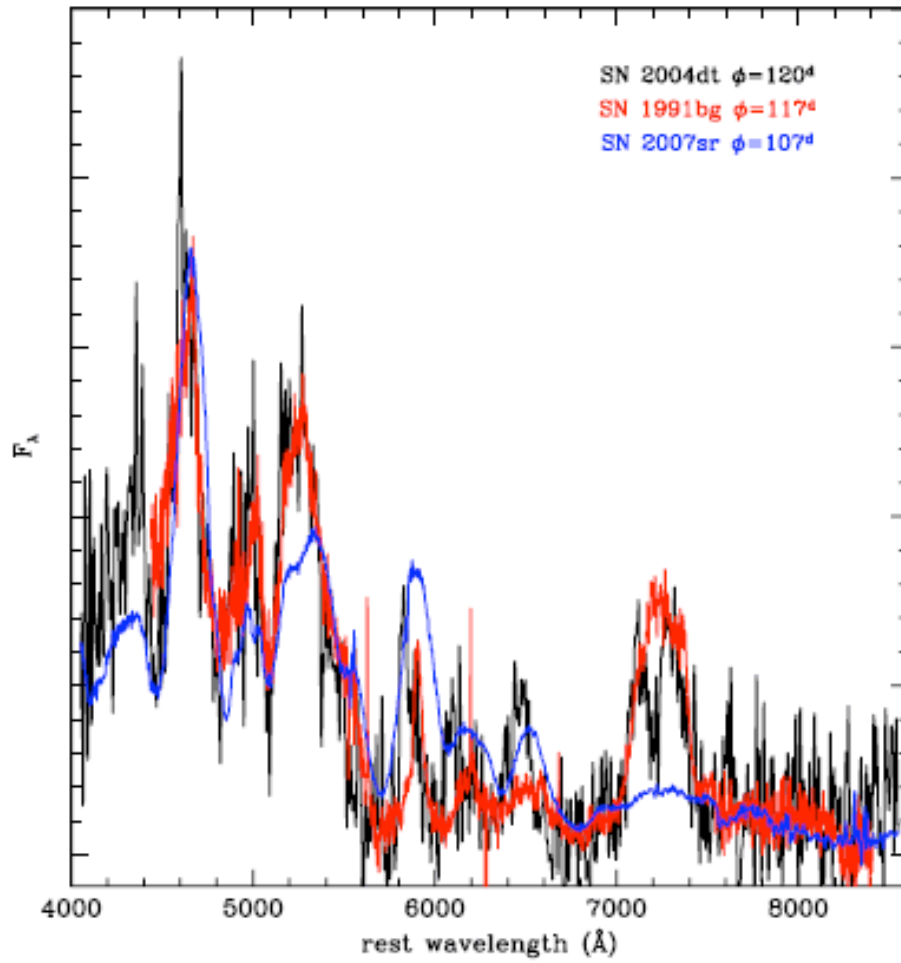
These two SNe would indeed have intrinsically different amounts of $M(^{56}\mathrm{Ni})$ and accordingly different luminosity. Because of different $M(^{56}\mathrm{Ni})$, $\Delta m_{15}(B)$ would be different if viewed from the same direction. Assuming that (1) $\Delta m_{15}(B)$ would be smaller and the luminosity is thus larger for LVG SN 1998bu than for HVG SN 2002bo, for a putative observer at the same direction, and that (2) $\Delta m_{15}(B)$ appears larger for an observer closer to the offset direction, as a viewing angle effect. Then, these two SNe would show similar $\Delta m_{15}(B)$ as observed, despite the intrinsic difference in luminosity, since the viewing direction is closer to the offset direction for SN 1998bu.

This effect would produce a scatter in the luminosity of SNe Ia, around the standard luminosity determined by $M(^{56}\mathrm{Ni})$. Pairs of SNe with similar $\Delta m_{15}(B)$, as a result of the viewing angle originating from SNe with different amounts of $M(^{56}\mathrm{Ni})$, are naturally

expected if we observe a large number of SNe Ia (Sup. Fig. 3) for the following two reasons: (1) SNe Ia do indeed show large variations in $M(^{56}\text{Ni})$, and (2) the viewing angles should display large variations.
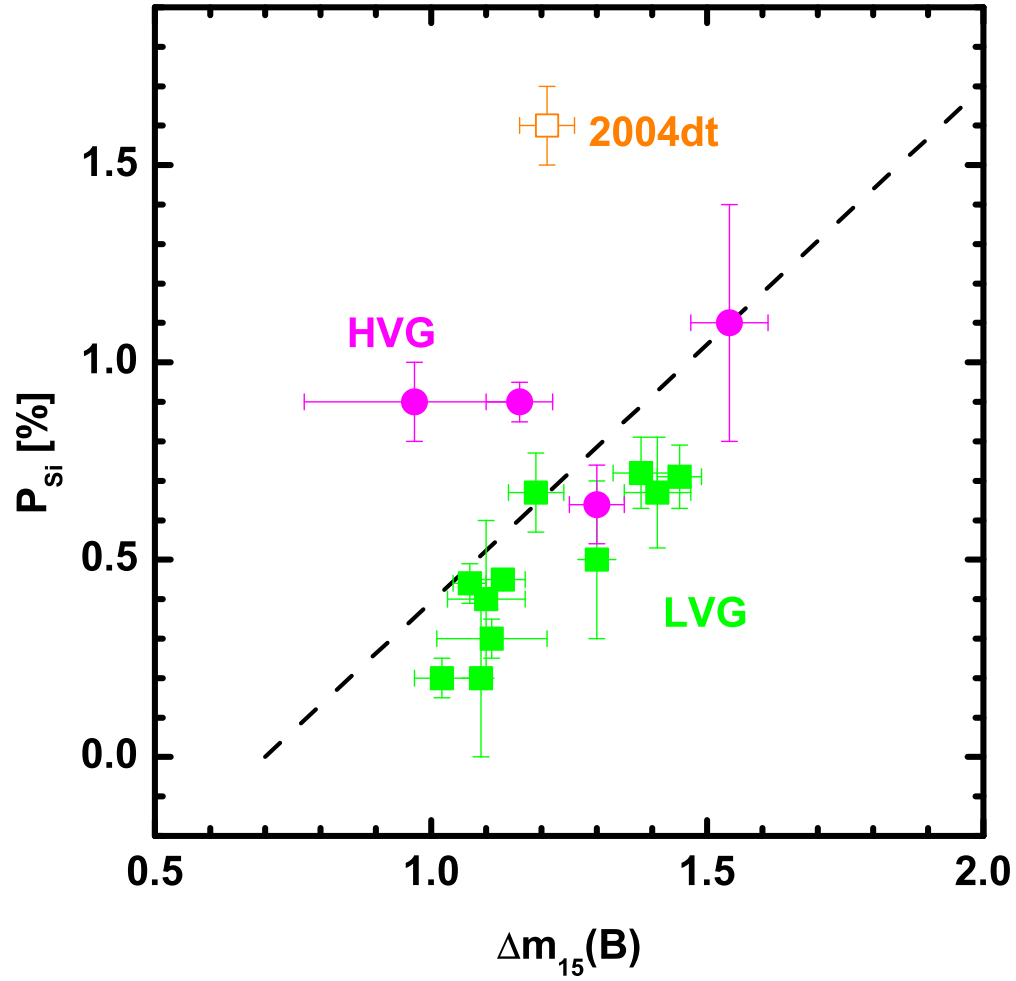
A question for this interpretation is whether any indication of such an effect is seen in the data. Supplementary Fig. 3 shows that there is no clear (but perhaps a marginal) correlation between $\Delta m_{15}(B)$ and v_{neb}. According to the prediction[5] of the viewing-angle effect on $\Delta m_{15}(B)$ for models similar to the one shown in the main text, the observed $\Delta m_{15}(B)$ could vary by ~ 0.4 mag depending on the direction to the observer (schematically shown in Sup. Fig. 3). This is smaller than the intrinsic variation in $\Delta m_{15}(B)$ for different $M(^{56}\text{Ni})$, and thus such an effect is difficult to notice in Supplementary Fig. 3, as is consistent with the low correlation in the present data. Any marginal correlation between $\Delta m_{15}(B)$ and v_{neb} may already hint that such an effect is indeed there, but a larger number of SNe Ia is necessary to test this possibility with statistical significance.

4 Supplementary Figure 1

Spectrum of SN 2004dt[29] at 120 days after B-band maximum, compared to those of

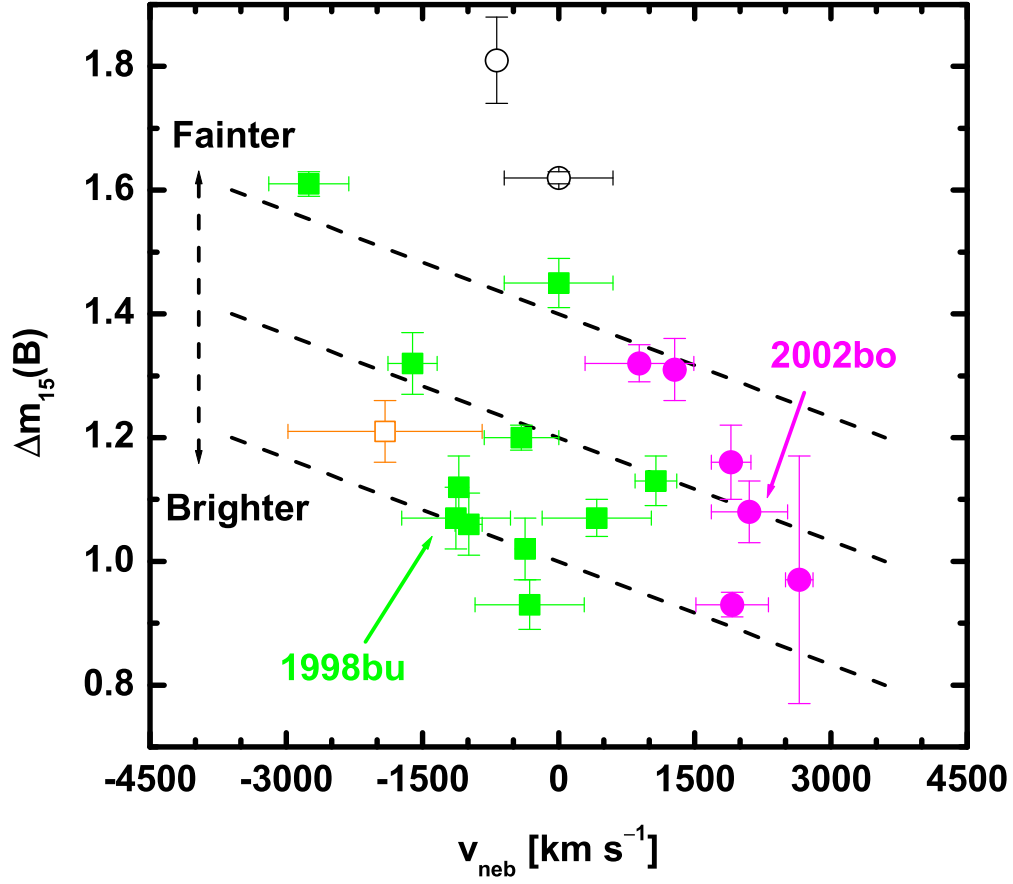the faint SN 1991bg[27] and of the normal HVG SN 2007sr at similar epochs.

5 Supplementary Figure 2

Si II λ6355 line polarization for SNe Ia, as a function of the decline-rate parameter[22,70,71]. The dashed line shows a linear fit to the data excluding SN 2004dt[22]. The colors of the symbols are the same as in Fig. 2 of the main text.

6 Supplementary Figure 3

The decline-rate parameter $\Delta m_{15}(B)$ versus the late-time emission-line velocity shift. The three dashed lines schematically illustrate the expected viewing angle effect on the decline-rate parameter, which would produce a ~ 0.4 mag difference in the observed $\Delta m_{15}(B)$ for an observer in the offset direction as opposed to the opposite direction[5]. The lines correspond to three hypothesized explosion configurations which are mutually different in $M(^{56}\text{Ni})$ and therefore in the intrinsic luminosity.

31. Phillips, M. M., et al., The Type Ia Supernova 1986G in NGC 5128 - Optical Photometry and Spectra, Pub. Astron. Soc. Pac., **99**, 592-605 (1987)

32. Cristiani, S., et al., The SN 1986 G in Centaurus A, Astron. Astrophys., **259**, 63-70 (1992)

33. Leibundgut, B., et al., Premaximum Observations of the Type Ia SN 1990N, Astrophys. J., **371**, L23-L26 (1991)

34. Gómez, G., López, R., Sánchez, F., The Canaris Type Ia Supernovae Archive (I), Astron. J., **112**, 2094-2109 (1996)

35. Patat, F., et al., The Type Ia Supernova 1994D in NGC 4526: The Early Phases, Mon. Not. R. Astron. Soc., **278**, 111-124 (1996)

36. Altavilla, G., et al., Cepheid Calibration of Type Ia Supernovae and The Hubble Constant, Mon. Not. R. Astron. Soc., **349**, 1344-1352 (2004)

37. Riess, A. G., et al., The Rise Time of Nearby Type Ia Supernovae, Astron. J., **118**, 2675-2688 (1999)

38. Branch, D., et al., Optical Spectra of The Type Ia Supernova 1998aq, Astron. J., **126**, 1489-1498 (2003)

39. Hernandez, M., et al., An Early-Time Infrared and Optical Study of The Type Ia Supernova 1998bu in M96, Mon. Not. R. Astron. Soc., **319**, 223-234 (2000)

40. Li, W., et al., The Unique Type Ia Supernova 2000cx in NGC 524, Pub. Astron. Soc. Pac., **113**, 1178-1204 (2001)

41. Patat, F., et al., Upper Limit for Circumstellar Gas around The Type Ia SN 2000cx,

Astron. Astrophys., **474**, 931-936 (2007)

42. Candia, P., et al., Optical and Infrared Photometry of the Unusual Type Ia Supernova 2000cx, Pub. Astron. Soc. Pac., **115**, 277-294 (2003)

43. Sollerman, J., et al., The Late-Time Light Curve of The Type Ia Supernova 2000cx, Astron. Astrophys., **428**, 555-568 (2004)

44. Krisciunas, K., et al., Optical and Infrared Photometry of the Nearby Type Ia Supernova 2001el, Astron. J., **125**, 166-180 (2003)

45. Wang, L., et al., Spectropolarimetry of SN 2001el in NGC 1448: Asphericity of a Normal Type Ia Supernova, Astrophys. J., **591**, 1110-1128 (2003)

46. Mattila, S., et al., Early and Late Time VLT Spectroscopy of SN 2001el - Progenitor Constraints for a Type Ia Supernova, Astron. Astrophys., **443**, 649-662 (2005)

47. Pignata, G., et al., Optical and Infrared Observations of SN 2002dj: Some Possible Common Properties of Fast-Expanding Type Ia Supernovae, Mon. Not. R. Astron. Soc., **388**, 971-990 (2008)

48. Pignata, G., et al., Photometric Observations of The Type Ia SN 2002er in UGC 10743, Mon. Not. R. Astron. Soc., **355**, 178-190 (2004)

49. Kotak, R., et al., Spectroscopy of The Type Ia Supernova SN 2002er: Days -11 to +215, Astron. Astrophys., **436**, 1021-1031 (2005)

50. Anupama, G. C., Sahu, D. K., Jose, J., Type Ia Supernova SN 2003du: Optical Observations, Astron. Astrophys., **429**, 667-676 (2005)

51. Stanishev, V., et al., SN 2003du: 480 days in The Life of a Normal Type Ia Supernova,

Astron. Astrophys., **469**, 645-661 (2007)

52. Leloudas, G., et al., The Normal Type Ia SN 2003hv out to Very Late Phases, Astron. Astrophys., **505**, 265-279 (2009)

53. Pastorello, A., ESC and KAIT Observations of The Transitional Type Ia SN 2004eo, Mon. Not. R. Astron. Soc., **377**, 1531-1552 (2007)

54. Hachinger, S., Mazzali, P.A., & Benetti, S., Exploring the Spectroscopic Diversity of Type Ia Supernovae, Mon. Not. R. Astron. Soc., **370**, 299-318 (2006)

55. Pastorello, A., et al., ESC Observations of SN 2005cf - I. Photometric Evolution of a Normal Type Ia Supernova, Mon. Not. R. Astron. Soc., **376**, 1301-1316 (2007)

56. Wang, X., et al., The Golden Standard Type Ia Supernova 2005cf: Observations from The Ultraviolet to The Near-Infrared Wavebands, Astrophys. J., **697**, 380-408 (2009)

57. Leonard, D. C., Constraining the Type Ia Supernova Progenitor: The Search for Hydrogen in Nebular Spectra, AIP Conference Proceedings, **937**, 311-315 (2007)

58. Garavini, G., et al., ESC Observations of SN 2005cf. II. Optical Spectroscopy and The High-Velocity Features, Astron. Astrophys., **471**, 527-535 (2007)

59. Wang, X. et al., Optical and Near-Infrared Observations of the Highly Reddened, Rapidly Expanding Type Ia Supernova SN 2006X in M100, Astrophys. J., **675**, 626-643 (2008)

60. Schweizer, F., et al., A New Distance to the Antennae Galaxies (NGC 4038/39) Based on The Type Ia Supernova 2007sr, Astron. J., **136**, 1482-1489 (2008)

61. Motohara, K., et al., The Asymmetric Explosion of Type Ia Supernovae as Seen from

Near-Infrared Observations, Astrophys. J., **652**, L101-L104 (2006)

62. Gerardy, C.L., et al., Signatures of Delayed Detonation, Asymmetry, and Electron Capture in the Mid-Infrared Spectra of Supernovae 2003hv and 2005df, Astrophys. J., **661**, 995-1012 (2007)

63. Filippenko, A.V., et al., The peculiar Type Ia SN 1991T - Detonation of a white dwarf?, Astrophys. J., **384**, L15-L18 (1992)

64. Phillips, M. M., et al., SN 1991T - Further evidence of the heterogeneous nature of type Ia supernovae, Astron. J., **103**, 1632-1637 (1992)

65. Pakmor, R., et al., Sub-Luminous Type Ia Supernovae from The Mergers of Equal-Mass White Dwarfs with Mass $\sim 0.9 M_\odot$, Nature, **463**, 61-64 (2010)

66. Tanaka, M., et al., The Outermost Ejecta of Type Ia Supernovae, Astrophys. J., **677**, 448-460 (2008)

67. Mazzali, P.A., Sauer, D.N., Pastorello, A., Benetti, S., & Hillebrandt, W., Abundance Stratification in Type Ia Supernovae - II. The Rapidly Declining, Spectroscopically Normal SN 2004eo, Mon. Not. R. Astron. Soc., **386**, 1897-1906 (2008)

68. Hachinger, S., Mazzali, P. A., Taubenberger, S., Pakmor, R., & Hillebrandt, W., Spectral Analysis of The 91bg-like Type Ia SN 2005bl: Low Luminosity, Low Velocities, Incomplete Burning, Mon. Not. R. Astron. Soc., **399**, 1238-1254 (2009)

69. Patat, F., Baade, D., Höflich, P., Maund, J. R., Wang, L., Wheeler, J. C., VLT Spectropolarimetry of The Fast Expanding Type Ia SN 2006X, Astron. Astrophys., **508**, 229-246 (2009)

70. Leonard, D.C., Li, W., Filippenko, A.V., Foley, R.J., & Chornock, R., Evidence for Spectropolarimetric Diversity in Type Ia Supernovae, Astrophys. J., **632**, 450-475 (2005)

71. Chornock, R., & Filippenko, A.V., Deviation from Axisymmetry Revealed by Line Polarization in the Normal Type Ia Supernova 2004S, Astron. J., **136**, 2227-2237 (2008)

72. Kasen, D., & Plewa, T., Detonating Failed Deflagration Model of Thermonuclear Supernovae. II. Comparison to Observations, Astrophys. J., **662**, 459-471 (2007)